Chapter-4

Wear Behavior of Ta-Coated 316L Stainless Steel

4.0 Introduction

Austenitic stainless steel type 316L SS is commonly used in implants, such as the knee, joint prosthesis, and bone fastening element, which are often impossible to replace in short periods **[112].** Therefore, they must be wear-resistant to be used safely and comfortably for many years. However, implants (i.e., knee replacement) are subjected to very different loads depending on the movement of the body; for this reason, surface hardness, alloy roughness, contact stresses, number of cycles, lubricants, and oxidation are the vital parameters for determining the wear performance caused by friction in body environment **[113].** The presence of a thin chromium-enriched oxide layer for protection on the 316L SS in the body environment is well-proven to strengthen corrosion resistance. However, 316L SS had many limitations, including pitting corrosion, which releases metal ions such as Cr, Ni, and Mo, weakening biocompatibility and compromising long-term performance [**114-115].** Deposited Ta films' lifespan and operational endurance are critical considerations in the aforementioned applications. Despite this, few investigations on the deposition of the thin layer of Ta on stainless steel have been conducted [**116**]**.** The literature review suggests correcting earlier research flaws and better understanding the relationship between film characteristics and Ta coatings' tribological and corrosive behavior. For implant development, the ASTM recommends type 316L rather than 316. As stated previously, the only variable in composition between 316L and 316 SS is the maximum carbon content, 0.03% and 0.08%, respectively. At room temperature, the Ni helps stabilize the Face-centered cubic crystal (FCC) structure, the austenitic phase, which helps strengthen the corrosion resistance **[117].** Both the Ni and Cr contents can influence the austenitic phase formation. The minimum amount of Ni needed

to maintain the austenitic phase is 10%. In the years to come, the need for orthopedic implants will keep on increasing, thus inspiring researchers and engineers to improve their surface integrity while enhancing their wear resistance. Consequently, implant surfaces must be modified with bioactive coatings to avoid releasing harmful ions that cause the loosening of joints due to wear [**117**]**.** A wide range of qualities exists based on heat treatment (annealing to create softer materials) or cold working for increased hardness and strength. As a result, the engineer must exercise caution while selecting materials of this nature. If a highly stressed and oxygen-depleted location, such as the interfaces under the screws of a bone fracture plate, even 316L SS can corrode inside the body **[118-121]**. Consequently, these stainless steels should be used as implant devices, i.e., fracture plates, screws, and hip nails. Anodization, passivation, and nitrogen implantation involving glow discharge are typical surface modification techniques for 316L SS to improve corrosion resistance, wear resistance, and fatigue strength **[118][120].**

Tantalum is a biomaterial that has been employed in medicine for a long time. The advantages of tantalum have attracted attention in extending its potential applications. Excellent biocompatibility and mechanical characteristics are two significant characteristics that are helpful for tissue regeneration of these materials introduced by novel manufacturing technology, such as the development of implants [**121**]. Future applications might involve the utilization of tantalum nanoparticles and hydrogel composites for the targeted delivery of medications to treat diseases, including cancer and degenerative disc disease [**122**]. Tantalum nanoparticles are known to be effective X-ray contrast agents with little cytotoxicity, including imaging of tissue composites, and are affordable and bioinert [**123-125**]. Tantalum has significant stability and healing capability, demonstrated through hip, knee, and spine surgeries in addition to the foot and ankle **[126].**

A porous tantalum implant and autologous iliac bone grafts were utilized to cure the patients. Furthermore, no histopathological proof exists that bone ingrowth into porous tantalum implants is insufficient **[127-129]**. Porous tantalum has a higher coefficient of friction than titanium fibre mesh, indicating that it facilitates better initial fixation. Porous tantalum has also been shown to increase the osteogenic potential and stimulate osteoblast proliferation more than titanium fibre mesh **[130-131]**. Lower bone loss could result from more significant bone formation in the areas around prosthetics due to the osteogenic impact of the porous tantalum and improved load transfer between the implant and bone due to early osseointegration **[132]**. To reduce prosthetic bone loss after THA, we thus anticipated that proximally coated stems with porous tantalum would be superior to those coated with titanium fibre mesh **[132].**

According to a literature review, Ta and its alloys have a long history of safe usage in implants and medical equipment because of their superior biological and material qualities. In particular, Ta and its alloys improve hemocompatibility for devices that come into direct contact with blood by preventing thrombosis and promoting endothelialization **[133]**. In contrast, porous Ta significantly improves osseointegration for devices that come into contact with bone by promoting Osteoconduction and osteogenesis. After one week, the patency rate (the fraction of open arteries) with the stainless-steel stents was 62%. The patency rate was 100% after a week if antithrombotic drugs were given. After one week, the Ta stents demonstrated 100% patency without needing antithrombotic drugs. Within seven days, the endothelium in both conditions covered the stents. The survival rates for the balloon angioplasty and Ta stent groups were 71.8% and 80.2% at the one-year follow-up. Furthermore, 100 patients had Ta stents placed in a randomized clinical trial by Garcia **[133]**, and no occurrences of sub-acute thrombosis by Rev Esp Cardiol were found.

According to these studies, the Ta stents stimulated endothelialization, which benefits long-term safety **[133]**.

In this study, 316L SS is coated with tantalum (Ta) with a thickness of 1.504µm, 3.809 µm, and 6.083µm duration of 15, 30, and 60 minutes, respectively, by the application of a DC magnetron sputtering system. Optical Microscopy characterized by Ta-coated and bare 316L SS, Scanning Electron Microscopy, Energy Dispersive X-ray Spectroscopy, and Atomic Force Microscopy after investigating wear and microhardness studies to find out the candidate biomaterial for higher durability without internal implant failure and effective performance (especially Ta-coated 316L SS) to the orthopedic applications.

4.1 Experimental details

4.1.1 Material and Sample Preparation

Austenitic stainless-steel type 316L was procured from M/s Mishra Dhatu Nigam Limited (MIDHANI), Hyderabad, India, with a dimension of $472 \times 775 \times 20\, mm$, and the received sample was converted into the required dimension of $20 \times 20 \times 2$ mm with the help of table moving Wire Electrical Discharge Machining Machine (WEDM) (Express cut Series-Ex4023C, India). **Table 4.1** shows the chemical composition of the as-received 316L SS alloy used in the experiment. After cutting the 316L SS through WEDM as per the required dimensions ($20 \times 20 \times 2\, mm$), the sample numbers are 04 for this wear study. Samples were mirror-polished before the deposition of the Ta coating using emery paper up to 1600 grit, followed by washing with distilled water and blow drying with hot air. The specimens were then ultrasonically cleaned with acetone for 30 minutes to achieve good adhesion with the coating. Optical Microscopy was used to check the substrate constantly to ensure the microstructure of the sample surface **[129][133].**

Table 4.1 The chemical composition of the as-received 316L SS

Material	C	Mn	S	P	Si	Cr	Ni	Mo
316L SS	0.03	1.39	0.005	0.003	0.015	17.5	13.6	2.27

4.1.2 Deposition of Tantalum

Tantalum thin films were deposited on 316L SS using a Direct Current Magnetron Sputtering (DCMS) technique. A thin-film Physical Vapor Deposition (PVD) coating in which an ionized gas molecule bombards a coating target material, causing atoms to 'Sputter' into the plasma; when the particles are vaporized, they condense and produce a thin coating on the substrate to coat. In the basic sputtering process, energetic ions released in glow discharge plasma bombard the target (cathode) plate. The target atoms' sputtering comes from the bombardment process, which can then condense as a thin layer on a substrate. Secondary electrons are emitted from the target surface due to the ion implantation, and these electrons play an important role in plasma control. Magnetrons take advantage of the fact that a magnetic field aligned with the target surface can restrict secondary electron transport to the target's vicinity. One pole of the magnets is situated at the target's central axis, while the second pole is generated by a ring of magnets around the target's outside edge. The probability of an ionization electron atom collision increases if electrons are confined in this technique. A magnetron's enhanced ionizing efficiency generates dense plasma in the target region. Consequently, the target is bombarded with more ions, leading to higher sputtering rates and, as an outcome, higher deposition rates on the substrate. Using a DC magnetron sputtering, the thin film was deposited onto stainless steel 316L with a high purity sputter tantalum target (99.95% Ta) with a diameter of 55.8mm and a thickness of 3.175 mm. **Table 3.3** (in Chapter 3) shows the DC Magnetron sputtering operational parameters for the coating Process. Before the

deposition operation, the sample was ultrasonically cleaned. Acetone was used in the cleaning process, followed by drying in pure Argon (Ag) gas flow. Each sample's deposition time was 15, 30, and 60 minutes. 316L SS substrates were placed right beneath the target's tracks inside the DC magnetron sputtering. Pre-sputtering was done 15 minutes before each layer deposition technique to clean the surface of the targets and eradicate all impurities and contaminants. A mass flow controller (MFC) was used to control the gas flow. The chamber was evacuated to a $5x\,10^{-4}$ Pa base pressure before the deposition process.

4.1.3 Microstructural Characterization

The 316L SS surface was examined using an optical microscope (OM, Leica Z6 APO.) Energy Dispersive X-ray Spectrometry (EDS) and Scanning Electron Microscopy (SEM, ZEISS MA 15/18, United Kingdom). SEM was used to analyze the surface morphology of the 316L SS. The chemical composition of the samples was assessed using EDS. Scanning Probe Microscope (NTEGRA Prima, NT-MDT Service & Logistics Ltd., Ireland) was used to analyze surface topography of as-received and Ta-coated 316L SS SPM physically raster-scans samples and gather information from the surface using a sharp point, and can detect a variety of signals in real-time with atomic or nano resolution, providing insights into structural properties.

4.1.4 Microhardness studies

Micro indentation Tester (MHT^3, Anton Paar Shimadzu Corporation, Kyoto, Japan) was used to determine the microhardness and elastic modulus of austenitic stainless-steel sample 316L SS and Ta-coated 316L SS at an applied load of 10 and 50mN at the acquisition rate of 10 Hz.

4.1.5 Wear studies

The pin-on-disc wear test is performed on a Ducom **(TR-701)** at 37°C in a simulated body fluid environment according to ASTM G99-95a**.** Very high purity (99.99%) AR grade chemicals have been used to prepare simulated body fluid (Alfa Aesar, US) at 7.4pH as per standard **[9].** With a normal load of 10, 20, and 40 N, zirconia pins with a diameter of 6 mm are used as counterparts. **Table 4.2** shows the **w**ear test parameters. **Fig. 4.1** presents the pin on the disc tribometer, in which parts assembly appears to be associated with the wear function and the actual device image. The counter face disc was made of hardened steel (EN31) with an Rc 60 hardness and a R_a 0.15 m surface roughness. Three types of plots are given from the data acquisition system: (a) Coefficient of friction against time, (b) Wear with load against the number of cycles, and (c) Wear rate against time.

The counter pin Zirconia (ZrO_2) mounted inside the holder was shifted upper side of the sample shown in **Fig. 4.1.** zirconia pins play a crucial role in wear testing by providing a challenging counter material with specific properties that help to evaluate the performance of materials in realistic wear conditions. Through zirconia pins as counter materials, can assess the coating's ability to resist wear, maintain low friction, and interact favorably with biological environments.

Table 4.2 Test parameters for wear studies

Test Parameters	
Pin material	Zirconia (ZrO_2)
Loading Profile	Constant
Profile Pattern	Linear
Pin dimensions (mm)	Φ6×20
Normal load (N)	10,20, 40
Speed (m/s)	20
No. of Cycle (s)	3600
Frequency (Hz)	1,2
Length (mm)	10

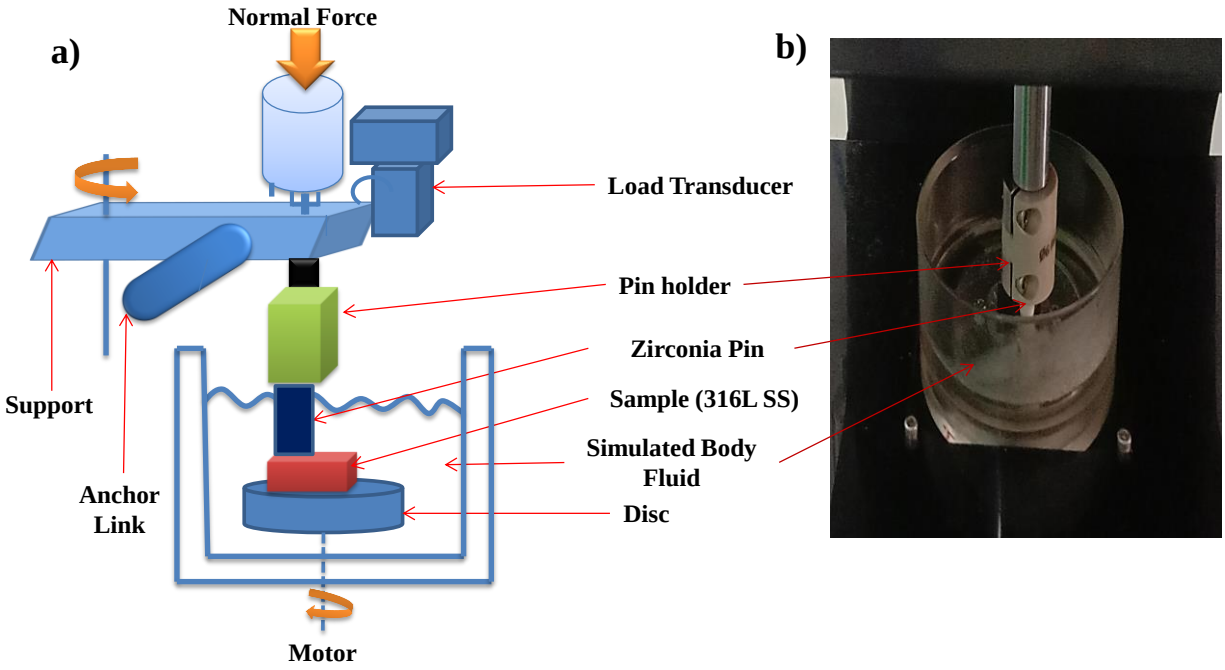

Fig. 4.1 Pin-on-disc tribometer **a)** Scheme of pin-on-disc assembly, **b)** device image.

4.2 Results and Discussion

4.2.1 Microstructural Characterization

A) Optical Microscopy: Figure 4.2 illustrates optical microscopy images of 316L SS surfaces, both bare and Ta coated, which have been polished and etched, reflecting light and providing contrast in the micrographs; a) polished 316L SS may obtain a clear image; grain boundaries can be seen when the surface is etched with aqua regia. b) Etched surface of Ta-coated 316L SS: Only uniform tantalum coating is shown when the specimen has no visible grains; only uniformity appears. The surface must be ground and polished using successively finer abrasives until it reaches a finish as near to ASTM E3 as possible for the material to reflect as much light as possible. Subsequently, sample preparation with a chemical reagent is followed by an etching procedure that selectively attacks and corrodes material at different rates. Due to changes in how much light

is reflected, these sections assist in contrasting the pictures, exposing the structure and size of grain boundaries, phases, inclusions, segregations, cracks, and pores **[136-138].**

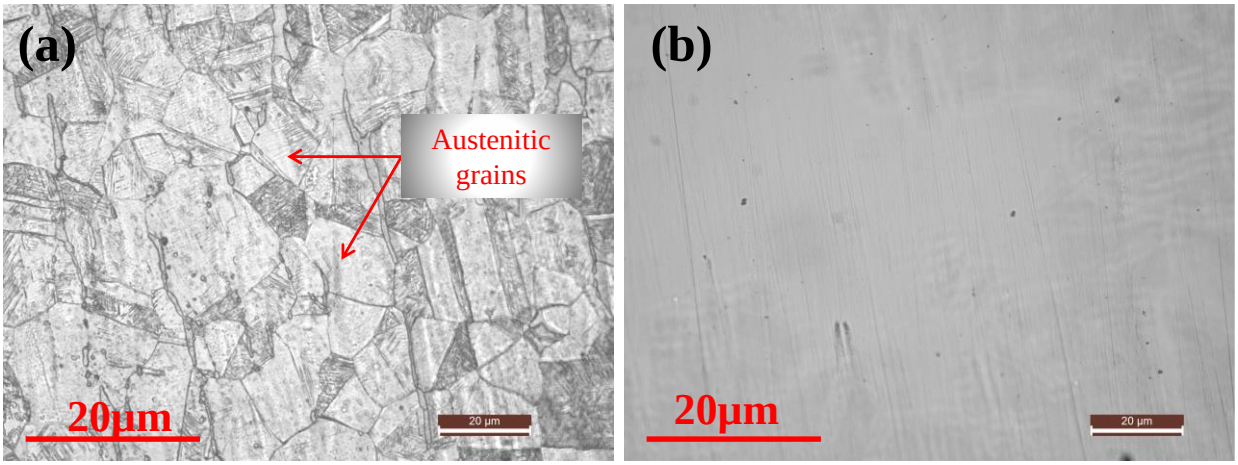

Fig. 4.2 Optical Microscopy images of 316L SS; **a)** Bare **b)** Ta-coated

B) Scanning Electron Microscopy (SEM):

The coating thicknesses with DC Magnetron Sputtering for all the specimens based on SEM analysis are reported. The thickness was uniform and improved as the coating deposition time increased. The coating thickness is obtained by cross-sectional cut after the tantalum coating over 316L SS and examined SEM (Except bare 316L SS). The average values of coating thickness after three iterations are reported. The SEM images of the cut coating are shown in **Fig. 4.3.** For a 15-minute deposition, the lowest thickness was 1.504 µm, while for a 60-minute deposition, the maximum thickness was 6.083 µm.

Fig. 4.5 illustrates SEM micrographs of the coated and bare 316L SS sections. The coating morphology for the metallic layers demonstrates a semi-columnar structure, as shown in these micrographs (Ta). The SEM micrographs exhibit the wear tracks developed during the sliding-contact experiments on substrates. It's best to observe the tribolayers formed for the debris produced during the sliding-contact tests and then consolidate them on the worn sections by linear

motion. The wear debris formed during the wear test at each load was collected and analyzed using SEM to investigate the behaviour mentioned above (Fig. 4.3(a–l)). Figures 4.3(a), 4.3(b), and 4.3(c) illustrate the wear track of bare 316L SS at a load from 10, 20, and 40N, respectively, which indicates the surface deformation is not more affected while applying the load of 10 to 20N and little change in deformation at a load of 40N.

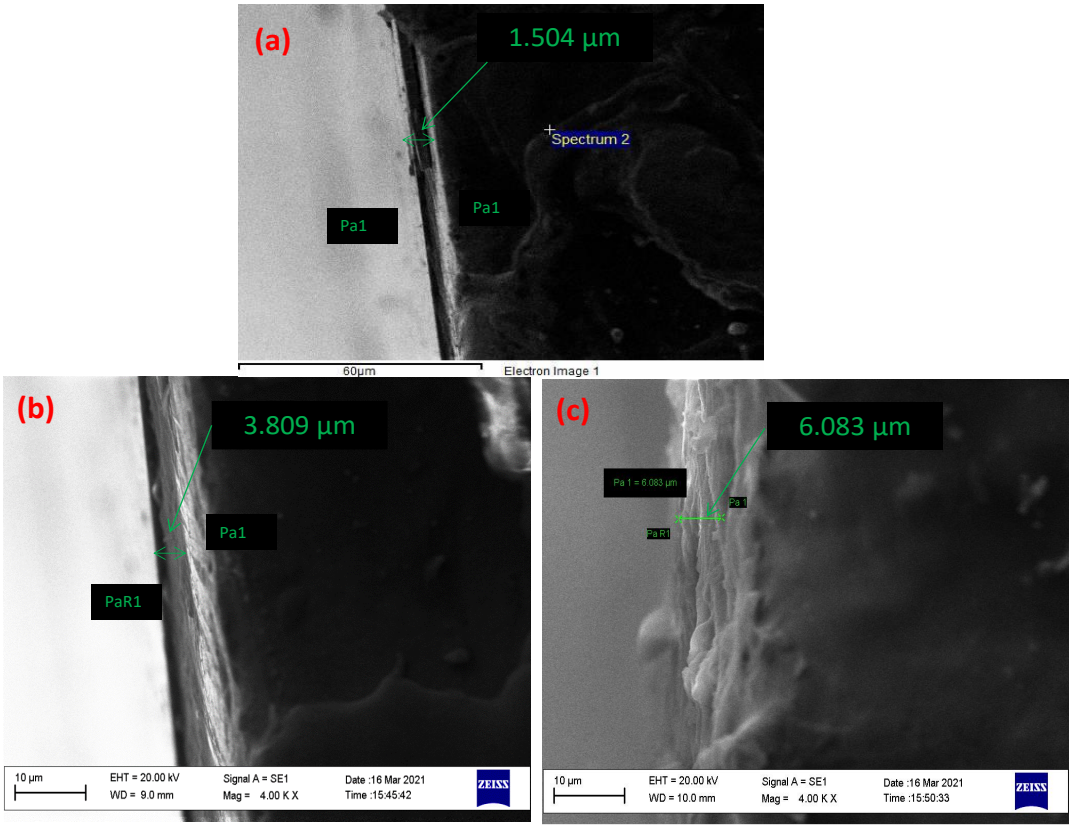

Fig. 4.3 SEM images of cross-section cut coating before the wear test **(a)** Ta-coated 316L SS for 15min. **(b)** Ta-coated 316L SS for 30min. **(c)** Ta-coated 316L SS for 60min.

However, in the case of Ta-coated 316L steel (from Fig. 3(d) to (l)), not many particles may be seen in the wear track, as shown by the arrowheads. Because the debris field is essential in order to prevent direct contact between native sample surfaces in relative motion, the COF increases. The bulk of the debris formed at 40N is approximately spherical, as seen in Figs. 4.3(f), 4.3(i), and

4.3(l), which can cause linear motion between the contact surfaces, resulting in a decrease in COF from a load of 40 N. It is reported a drop in COF for mild steel is related to the rolling of debris particles. Similarly, **[28]** demonstrated a reduction in COF for harmonic structured austenitic stainless steel due to the rotation of wear particles. The Hertzian contact pressure and contact area diameter were determined using Eqs. (1), and (2) at a load of 2–10 N to investigate the correlation between the form and size of worn trash and the applied load **[124-125].**

$$a = \sqrt[3]{\frac{3f}{8}\frac{\frac{(1-\mu^1)}{E_1}+\frac{(1-\mu^2)}{E_2}}{\frac{1}{d^1}+\frac{1}{d^2}}} \quad (1)$$

$$P_{max} = \frac{3f}{2\pi a^2} \quad (2)$$

Where F is the normal load, A is the Hertzian contact radius, and E1 and E2 are the elastic moduli of the ball and the sample, respectively. The diameters of the ball and the sample are d1 and d2, the Poisson's ratios of the ball and the sample are μ1, and μ2 and P_{max} is the contact pressure.

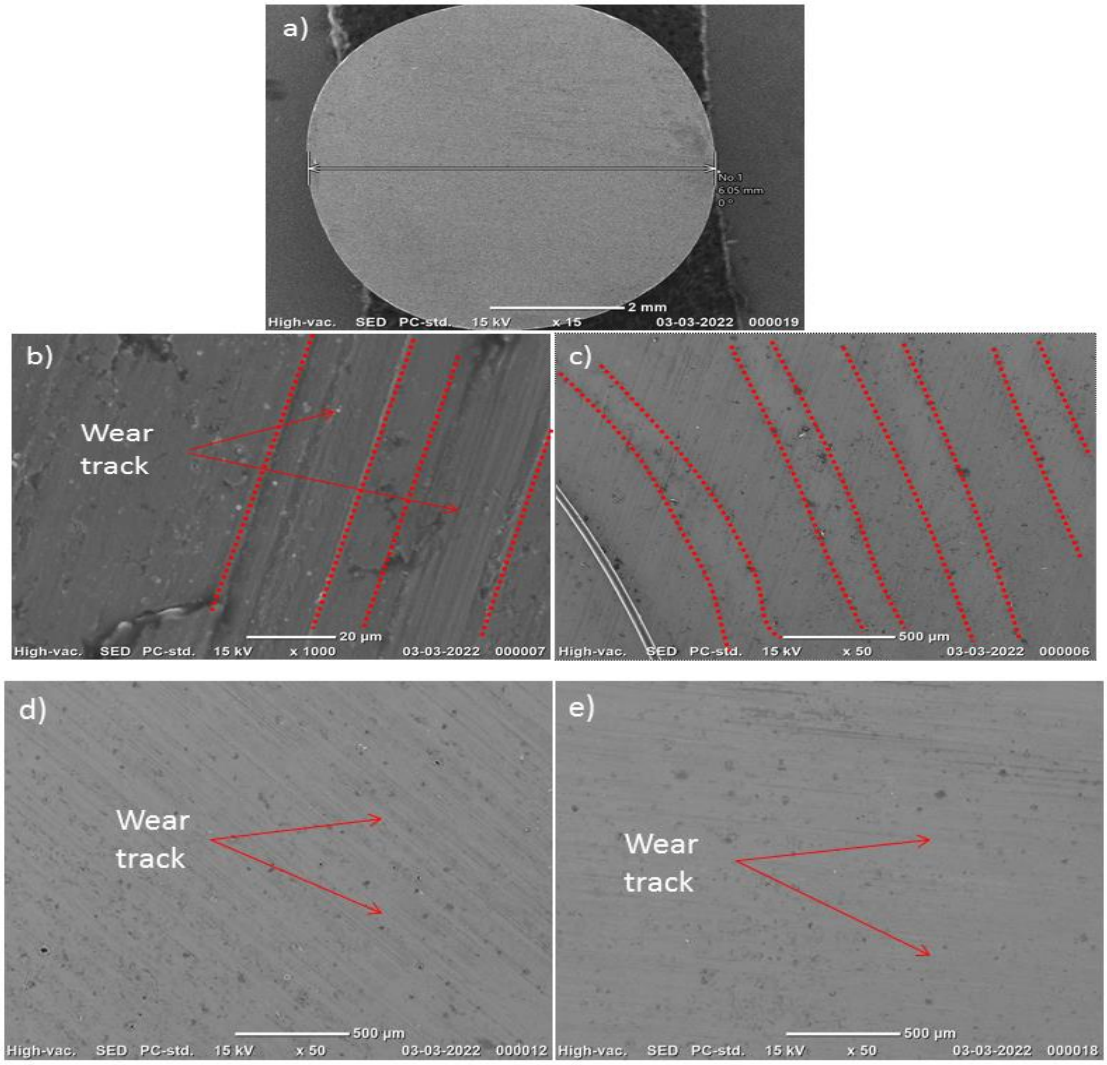

Fig. 4.4 SEM images of zirconia pin after wear test; **a)** pin diameter **b)** bare 316L SS treated pin **c)** Ta coated for 15min 316L SS treated pin **d)** Ta coated for 30min 316L SS treated pin **e)** Ta coated for 60min 316L SS treated pin.

The proportion of the generated wear debris at 10 N (Figs. 4.3(a), (d), (g), and (j)) is of significantly smaller size for all specimens, apparently due to lower contact stress values at the increased load. Because fine and coarse grains coexist, the hardness of 316L stainless steel is uniform. Thus, the size and shape of debris produced in these places will be distinctly diverse from debris produced by other steels. **Figure 4.4** shows the SEM images of the zirconia pin after the wear test, as the counter zirconia pin could roll over adequately between the continuously moving surfaces. It might

be attributed to the harmonic steel's COF increasing substantially when the load increases from 5 N to 10 N; for the bare stainless steel 316L, and it is found a similar phenomenon in COF variation with load has been reported **[139-140].**

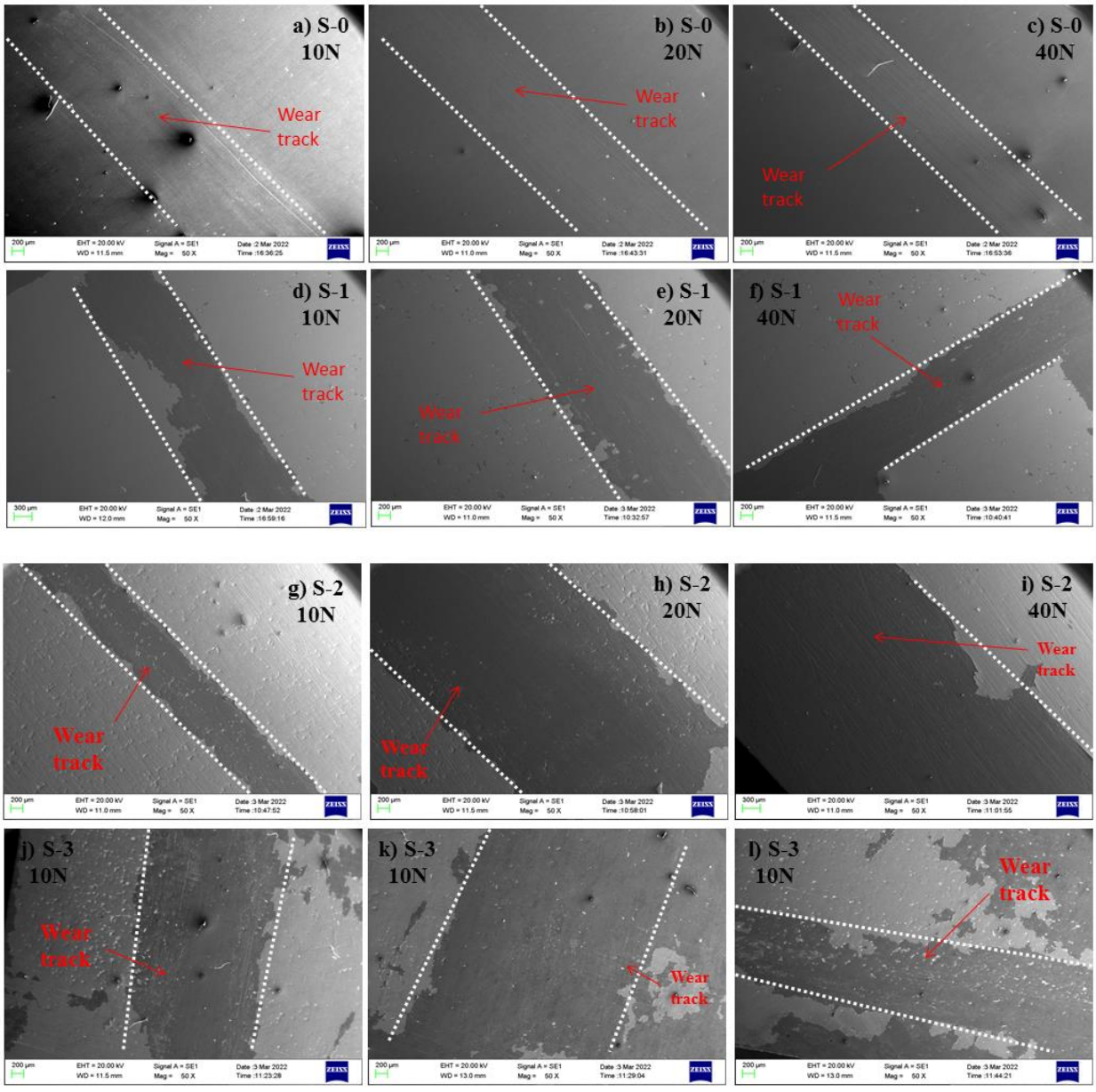

Fig. 4.5 SEM images after wear test of bare and tantalum coated samples; (**a-c)** Bare 316L SS at 10N, 20N, and 40N (**d-f)** Ta coated 316L SS for 15min. at 10N, 20N, and 40N (**g-i)** Ta coated 316L SS for 30min. at 10N, 20N, and 40N **j-l)** Ta coated 316L SS for 60min. at 10N, 20N, and 40N.

C) Energy Dispersive Spectroscopy (EDS): The EDS analyses of the bare and Ta-coated 316 L samples were carried out for all the samples. It is observed that Cr, Mn, Ni, C, and Mo elements were present on the surface of 316L SS, as shown in **Fig. 4.6(a),** and Cr, Mn, Ni, C, Mo, and Ta elements appeared in **Fig. 4.6(b-d).** All samples were subjected to an EDS examination on the upper side surface. In the maximum locations, the findings revealed Ta contents in Ta-coated samples. In certain places, as illustrated in **Fig. 4.6(b-d),** a significant amount of tantalum was detected. The oxygen concentration of the stainless steel 316L did not match the material composition. The material constituents were dispersed in a non-homogeneous approach. It was observed that the components in the build plate's central have less nickel and chromium than the rest.

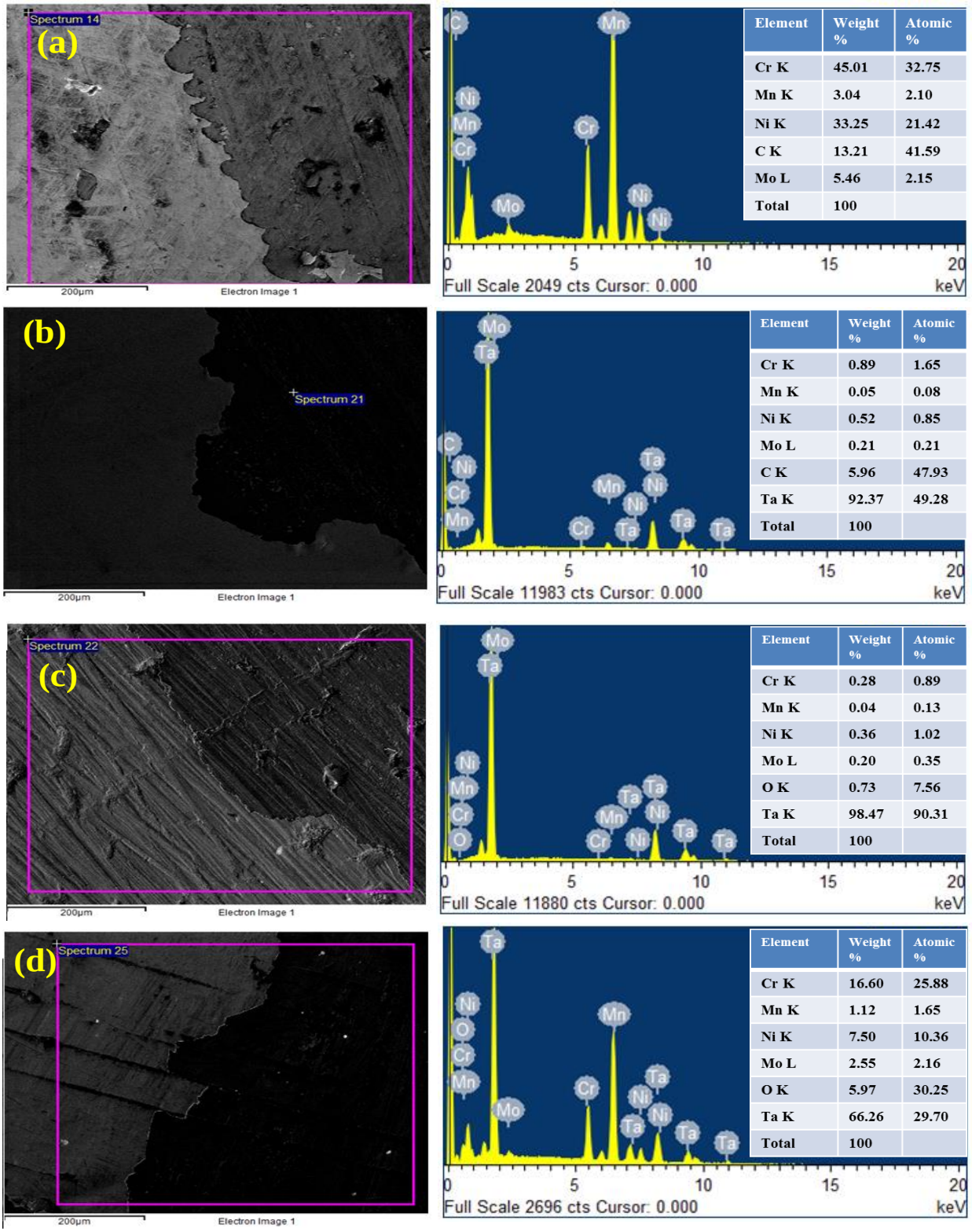

Fig. 4.6 EDS images of bare and Ta coated 316L SS; a) bare 316L SS b) Ta coated for 15min 316L SS c) Ta coated for 30min 316L SS d) Ta coated for 60min 316L SS.

D) Atomic Force Microscopy (AFM)

Atomic Force Microscopy is a kind of Scanning Probe Microscopy, a set of techniques for determining the topography and characteristics of surfaces at the atomic level. The AFM probes the surface of a material with a sharp tip that is a few microns long and often less than 100 microns in diameter. At the outer surface is the tip of a cantilever that is 100 to 200 m long. The forces between the tip and the sample surface cause the cantilever to bend or deflect. A detector monitors the cantilever deflection whenever the tip is scanned over the sample or the sample is scanned under the tip.

Table 4.3 Roughness results of bare and Ta-coated 316L SS

Sample Name	**Sample Evaluation Area (μm^2)**	**Ra (nm)**	**Rq (nm)**
316L SS (Bare)	2500.195±0.112	9.213±0.135	17.123±0.125
316L SS (15 min)	2500.195±0.126	11.658±0.112	15.871±0.116
316L SS (30 min)	2500.195±0.138	41.762±0.101	52.895±0.127
316L SS (60 min)	2500.195±0.142	46.425±0.120	55.260±0.147

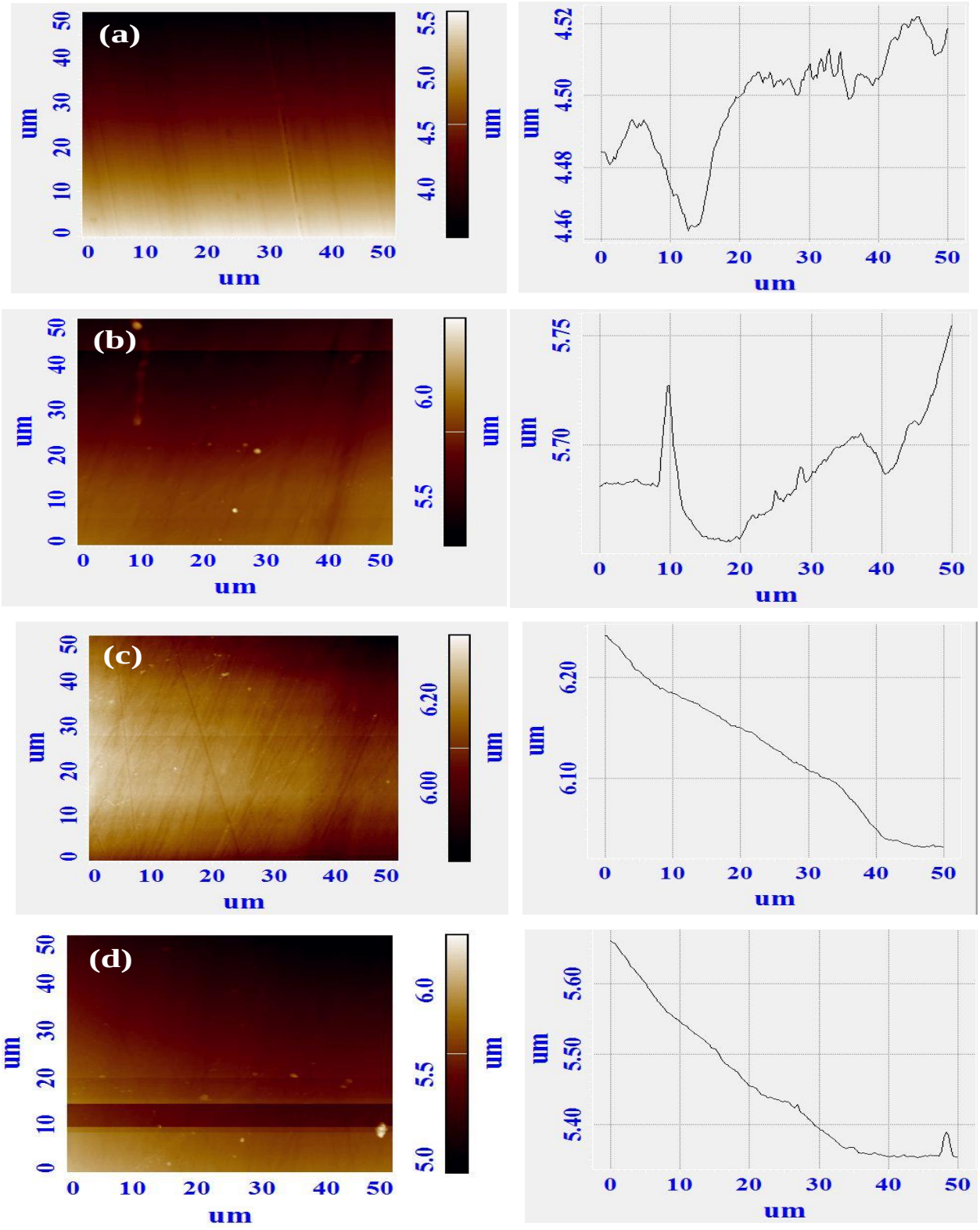

Fig. 4.7 Two-dimensional AFM images of the 316L SS; a) Bare b) Ta-coated (15min) c) Ta-coated (30min) d) Ta-coated (60min)

Figure 4.7 shows the two-dimensional AFM images of the 316L SS. Surface profile parameters to quantitative analysis of AFM data image of the surface topography are essential to comprehend the morphology of a surface. The average standard deviation values of five readings were taken. To avoid repeatability, only one graph has been reported. In each profile line, the topography matrix data needs to be processed (2D), including across all profiles, whereas if the analysis is to be expanded to the surface (3D). The amplitude parameters, also known as height parameters, are the primary characteristics used to characterize the surface topography. The most commonly utilized amplitude parameters are (R_a) and (R_q). As seen in section 2, the last one is beneficial for evaluating temporal variations in constructing new surface and spatial differences when studying the surface characteristics at different scales. This is because substantial deviations from the mean line make this parameter more sensitive.

To determine the fit of the Rq values, the height points must be uniformly distributed according to a normal distribution curve **[141].** The measurement should be repeated if the average roughness and RMS roughness of a given height profile in a surface mismatch. **Table 4.3** shows the Roughness results of bare and Ta-coated 316L SS. When an image contains many peaks and valleys, the Ra and Rq values are considerably affected; hence, calculating the average peak-to-valley difference is preferable. The height parameter peak-to-valley was utilized to measure the periodic structure of the films in the experiments **[141-142].** The tapping mode was performed to observe the periodic pattern on the surface and the periodic peaks that accumulated in pairs for the calculations.

Figure 4.8 shows the three-dimensional AFM topography of Ta-coated 316L SS over a 2500.195 μm^2 scan region. On the substrate, the image revealed a columnar growth of Ta in **Fig 4.8(b-d)**. The film's microstructure was enhanced by increasing the annealing temperature **[143].** The

regions with the highest height gradients correspond to the darkest and brightest regions. The brightness of a region is proportional to its granular microstructure height and flat texture, composed of spherical particles. The Ta-coated 316L SS substrate's RMS roughness value was determined and found to be about 10.6 nm. The line profile shows the height significance or characteristic feature of the pores' depth**.** The line profile also suggests that the films have a lot of nanoscale or sub-micrometre pores **[144].**

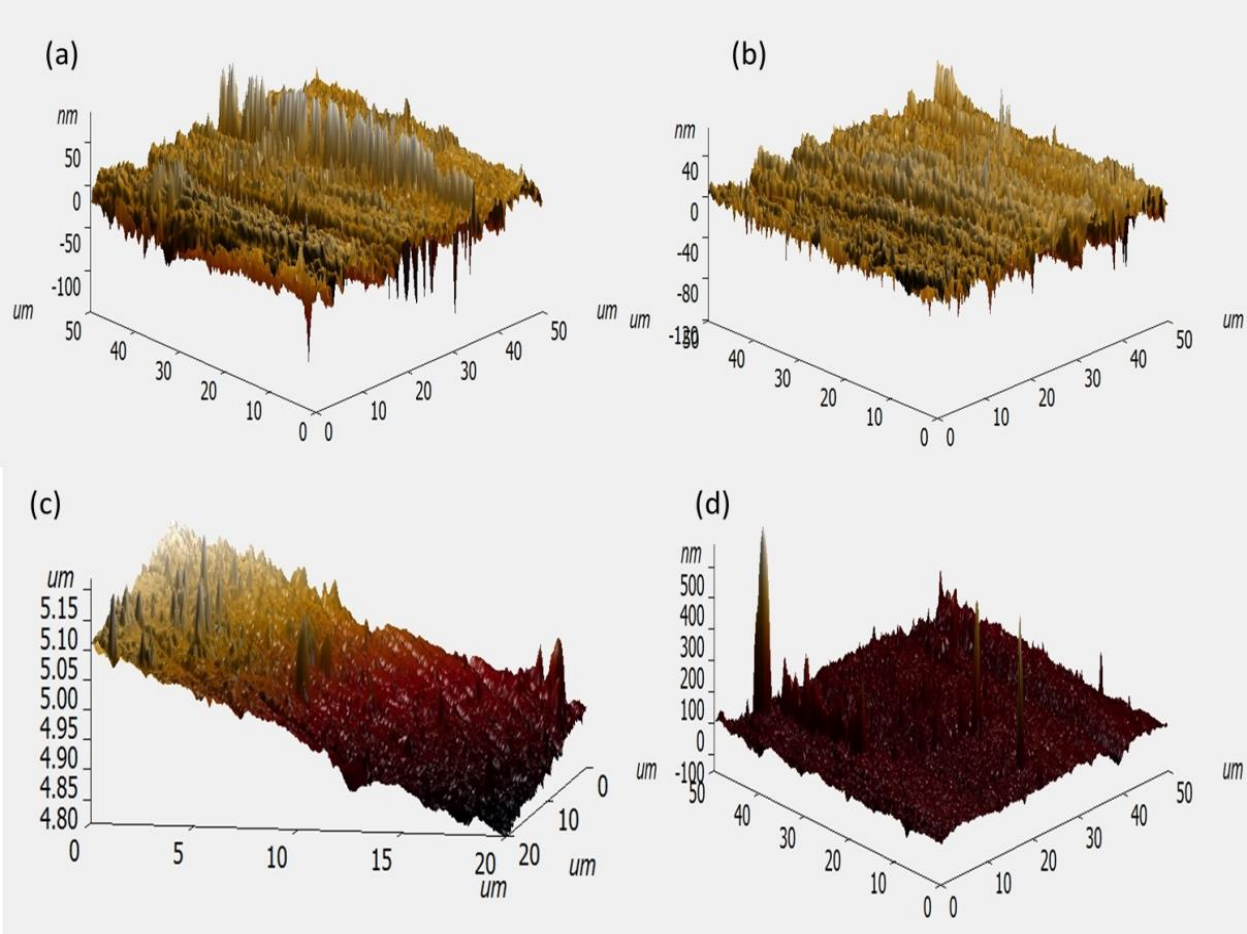

Fig. 4.8 Three-dimensional AFM images of the 316L SS; a) Bare b) Ta-coated (15min) c) Ta-coated (30min) d) Ta-coated (60min)

4.3 Microhardness studies

For each sample, six indentations were recorded at different positions on the coated and bare surface of 316L SS to prevent random error, and the average results were reported. The recorded load-displacement curves were used to determine elastic modulus and hardness. The indenter tip was then used to scan the indentation impressions in place. **Table 4.4** shows the test parameters for bare and Ta-coated 316L SS microhardness. The indentation load is divided by the estimated contact area of the indentation to calculate micro-indentation. It is the maximum pressure that a substance can withstand when loaded. Hardness at the peak load may be calculated using the load-displacement curve as follows:

$$H = \frac{P_{max}}{A} \quad (1)$$

P_{max} denotes the maximum load, while A denotes the expected contact area. The projected contact area of an indenter with a defined shape, such as the Berkovich tip employed in this work, is a function of contact depth determined in situ by the nanoindenter during indentation **[145].** As a result, the indentation displacement may be used to measure and compute the projected area A. The following is a geometry-independent relationship involving contact area and elastic modulus:

$$s = 2\beta\sqrt{\frac{A}{\pi}}\,E_r \quad (2)$$

Where β is a constant that depends on the indenter's geometry (β=1.034 for a Berkovich indenter), and E_r is the reduced elastic modulus that accounts for elastic deformation in both the sample and the indenter **[145].**

$$\frac{1}{E_r} = \frac{1-v^2}{E} + \frac{1-v_i^2}{E_i} \quad (3)$$

The elastic modulus and Poisson's ratio for the sample are E and v, respectively, whereas E_i and v_i are the same for the indenter.

Fig. 4.9 shows sample load-displacement curves, indentations made at 20 and 50 mN, and peak indentation load on 316L SS and Ta-coated 316L SS. The unloading curve's lowest indentation depth and maximum slope are observed in bare 316L SS, followed by Ta-coated. All around, indentation marks of bare and a small pile-up were visible. Both bare and coated specimens' hardness and elastic modulus were calculated at the depth presented in **Table 4.4** using six micro-indentations. The tip is Vickers type and loading/unloading at a rate of 100.00 mN/min. Plots were reported. **Figure 4.10** represents the Vickers hardness versus no. of indentation for bare and Ta-coated 316L SS.

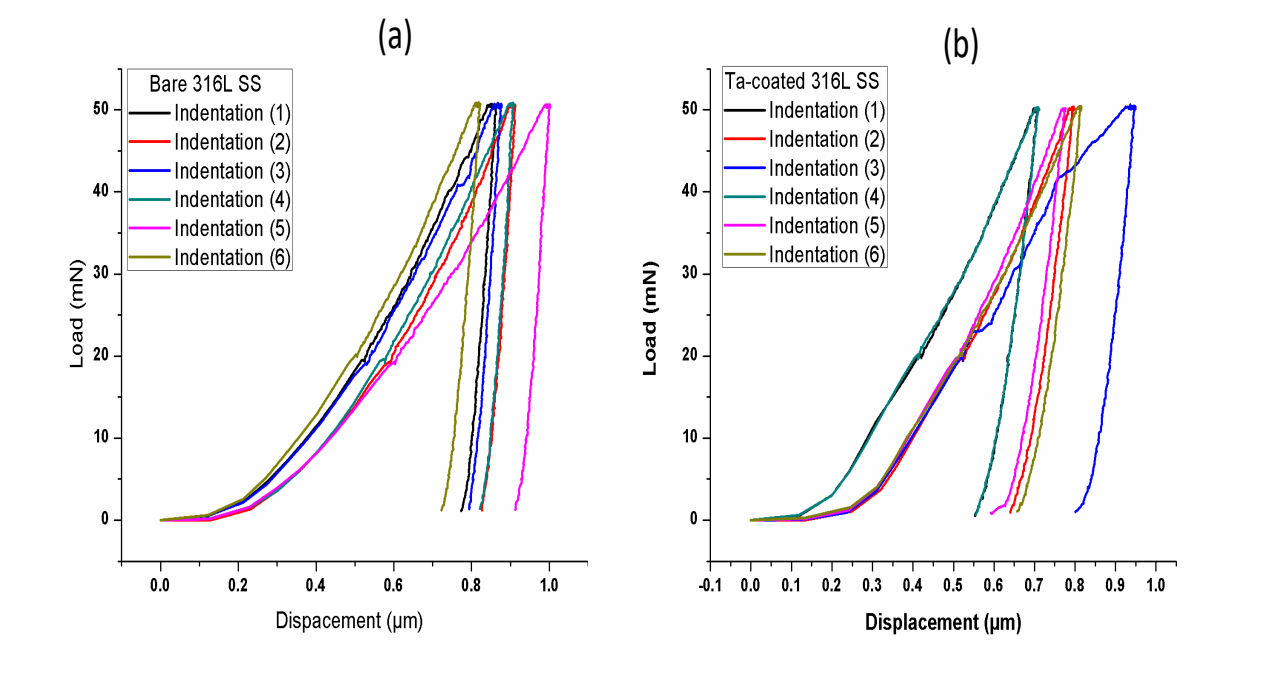

Fig. 4.9 Load and Displacement curves for 316l SS (a) Bare (b) Ta-coated

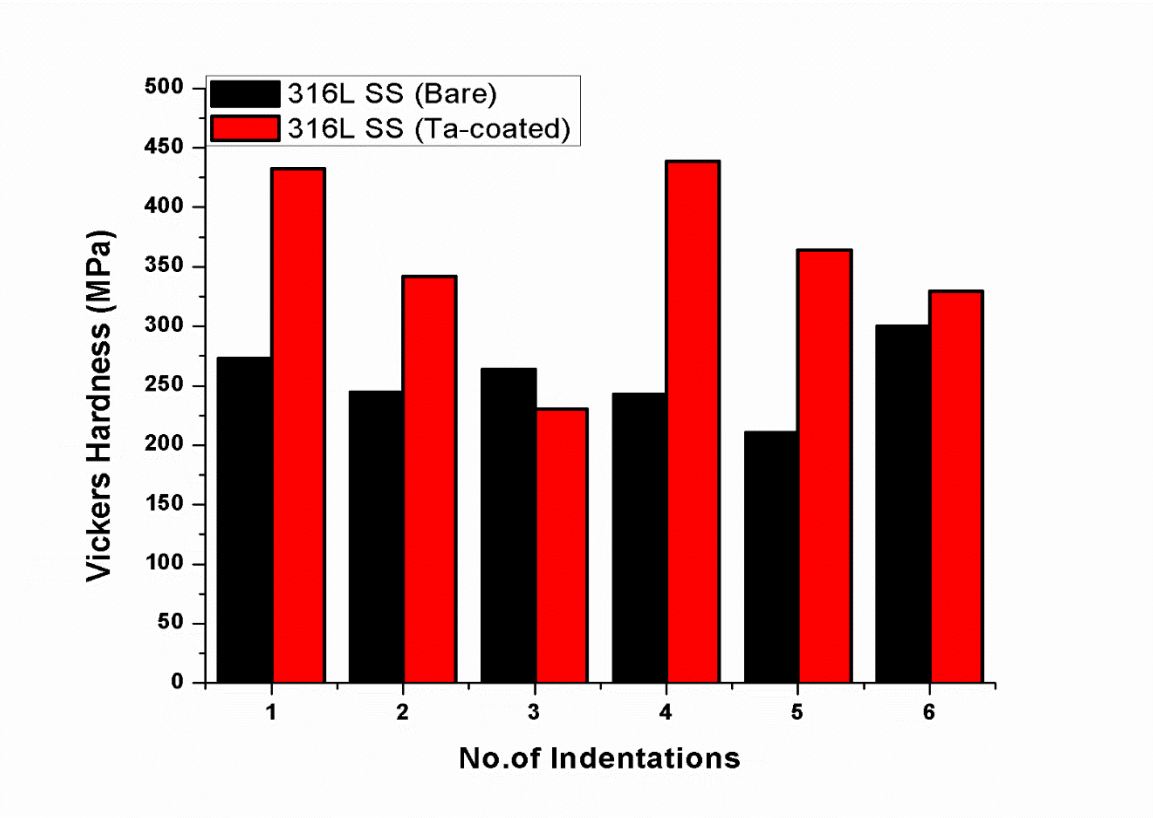

Fig. 4.10 Vickers hardness of bare and Ta-coated 316L SS

Figure 4.11 shows the modulus of Elasticity, Hardness, and Counts curves for 316L SS. The elastic modulus and hardness values are obtained from the load-displacement curves using standard techniques **[146].** The elastic modulus and hardness of bare and coated 316L SS were determined as a function of depth using many partial loading/unloading nano-indentations. The results of the testing, as well as the hardness and elastic modulus values obtained from the load-displacement curves using standard methods **[145-146].**

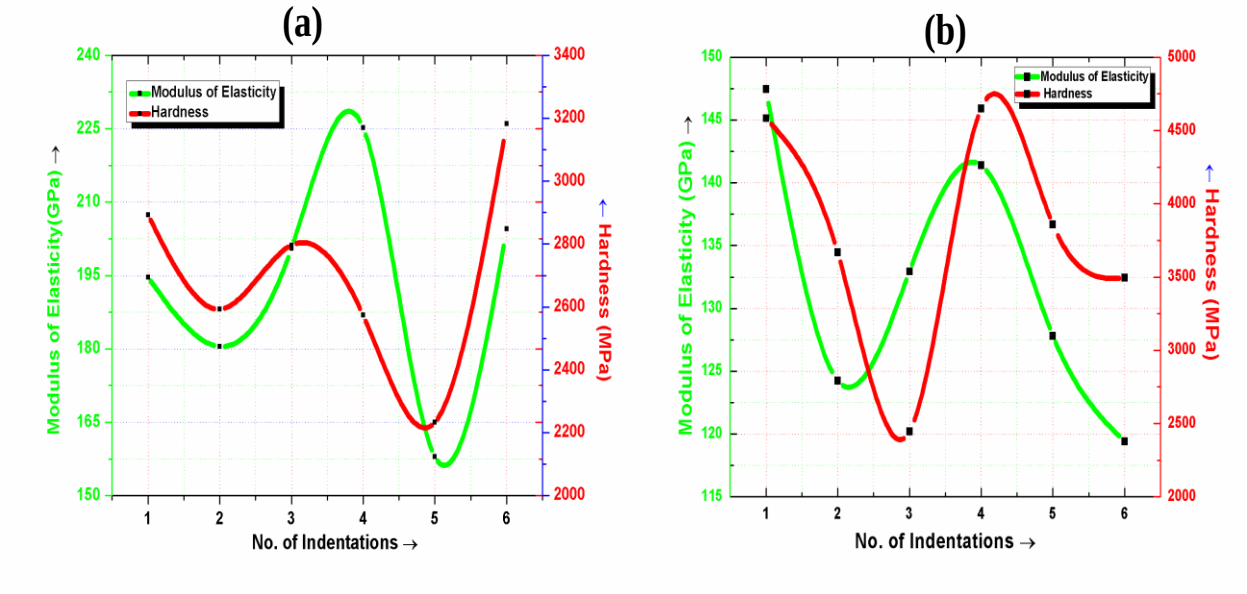

Fig. 4.11 Modulus of Elasticity, Hardness, and No. Of indentation curves for 316L SS (a) Bare (b) Ta-coated

Figure 4.12 shows the micro indentation images of 316L SS. The MHT^3 standard indentation rate parameters for bare and coated samples were linear loading maximum load 50mN, acquisition rate 10Hz, loading rate 100mN/min., unloading rate 100mN/min., and pause for the 20s. Based on the microhardness test (No. of Indentation = 06) for bare and Ta-coated 316L SS, it concluded that after coating of tantalum over 316L SS, Hardness increases (Avg. = 3783.28 MPa) and Modulus of Elasticity decreases (Avg.= 132.16 GPa). Indentation depth of height (h) for bare 316L SS was obtained (Avg. = 0.83 µm), and for the Ta-coated sample was (Avg. = 0.69 µm). That indicates that coated samples are taken with minimum indentation depth due to coating thickness.

Table 4.4 Test parameters and results at the rate of 10Hz microhardness for bare and Ta-coated 316L SS.

Test Parameters					Hardness (MPa)		Modulus of Elasticity (GPa)	
No. of Indentation	Load (mN)	Poisson's ratio	Depth of indentation Bare (µm)	Depth of indentation Coated(µm)	Ta-Coated	Bare	Ta-Coated	Bare
1	50,20	0.3	0.80	0.61	4583.5	2892.5	147.47	194.68
2	50,20	0.3	0.85	0.69	3667.2	2592.4	124.26	180.49
3	50,20	0.3	0.81	0.87	2444.8	2796.4	132.94	200.55
4	50,20	0.3	0.85	0.60	4651.4	2574.2	141.1	225.22
5	50,20	0.3	0.93	0.67	3858.8	2233.2	127.82	157.96
6	50,20	0.3	0.76	0.71	3494	3182.1	119.42	204.57
				Average	3783.28	2711.80	132.16	193.91

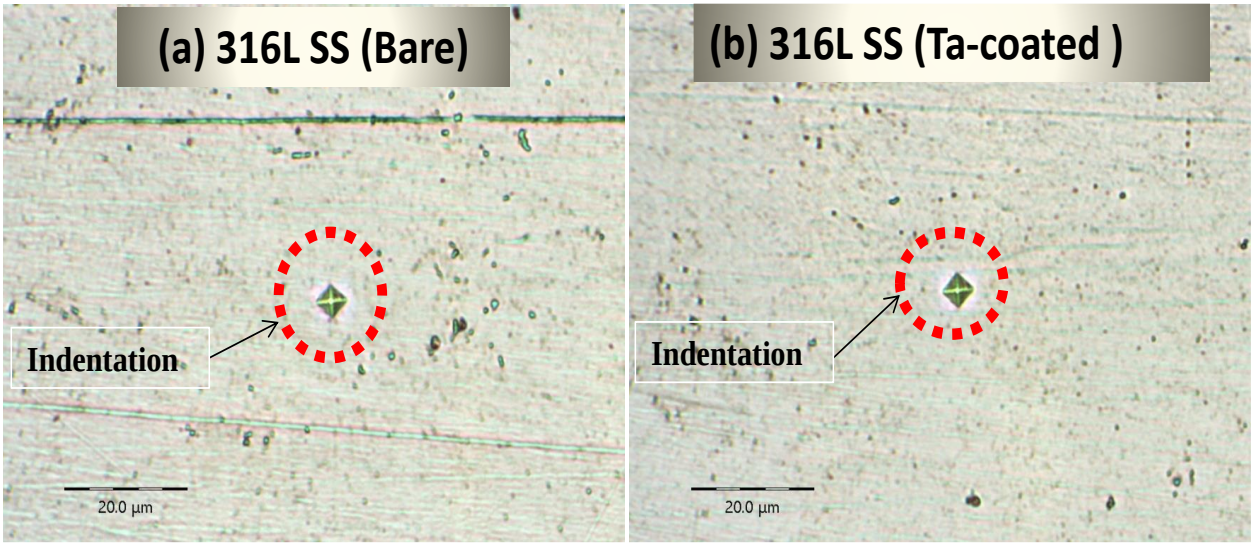

Fig. 4.12 Micro indentation images of 316L SS; a) Bare 316L SS b) Ta coated

4.4 Wear studies

The wear properties of Ta-coated 316L SS were studied using a pin-on-disk test and compared to the bare substrate. In the experiment, the parameters such as time (60min.), temperature (37°C), and frequency are constant, and loads vary throughout all the experiments. **Table 4.5** shows the wear test parameters; the weight loss of the samples was determined by weighing each before and after the wear test on a digital balance (Model No. K-BA 200, K-Roy instruments India) with 0.0001g accuracy. **Figure 4.13** shows the experimental wear test images of worn surfaces of bare and Ta-coated 316L SS. Each bare and Ta-coated 316L SS sample's weight loss and coefficient of friction (COF) are recorded. These samples' volume loss and wear rates are calculated using Archard's equations.

As tested at 10 to 40N load, the weight loss of both bare and coated 316L substantially was negligible based on **Table 4.5**, and the wear throughout the test seems to be the same based on the observed performance. The weight loss in samples was 0.18% max. and 0.01% min., which was observed in AISI 316L samples **[133].**

Based on the microhardness results reported above, it can be observed that, in addition to increasing the microhardness of Ta-coated 316L SS compared to bare 316L SS, it also improves its wear resistance. The treated surfaces are more rigid than the turned ones and, thus, more friction-resistant. This follows Archard's law, which indicates that the higher the microhardness, the more resistant the material is to wear. The pressure was obtained through the Hertzian contact pressure ($P = 4F/\pi D^2$) and got the corresponding pressures 0.003, 0.006, and 0.012 MPa at 10, 20, and 40 N load, respectively.

Table 4.5 Wear rate results for bare and Ta-coated samples at different parameters.

Sample/ Parameters	Weight loss (g)	Volume loss (mm^3)	Track length (m)	Density (g/cm^3)	Load (N)	Wear rate (mm^3/Nm)	Wear rate (mm^3/Nm) ($*10^{-5}$)
Bare	0.0004	0.00005	10	8	10	0.0005	50.00
	0.0009	0.0001125	10	8	20	0.0005625	56.25
	0.0020	0.00025	10	8	40	0.000625	62.50
15min	0.00009	5.625E-06	10	16	10	0.00005625	5.62
	0.0002	0.0000125	10	16	20	0.0000625	6.25
	0.00042	0.00002625	10	16	40	0.000065625	6.56
30min	0.00007	4.375E-06	10	16	10	0.00004375	4.37
	0.00015	9.375E-06	10	16	20	0.000046875	4.68
	0.00031	1.9375E-05	10	16	40	4.84375E-05	4.84
60min	0.00005	3.125E-06	10	16	10	0.00003125	3.12
	0.00011	6.875E-06	10	16	20	0.000034375	3.43
	0.00024	0.000015	10	16	40	0.0000375	3.75

Friction Coefficient: For different load and sliding speeds, the COF performances against the time result for bare and coated 316L SS are presented in **Fig. 4.14,** in which Fig.4.14(a) describes bare 316L SS, which indicates that COF lower (0.25) at an applied load of 20N and higher (0.55) at 40N load. Fig. 4.14(b) shows the 15min. Ta coated clearly indicates that COF is higher (0.50) at 40N load and lower (0.1) at 10N. Higher COF (0.45) was predicted at 40N for 30min. Ta-coated sample and lower (0.23) at 40N and 60min. Ta-coated samples have higher COF (0.07) at a load of 40N and lower (0.20) at a load of 10N. There is a short running-in phase (0-10 m) at the start of the testing, during which the tribological pairs are coupled. Surfaces may interface more easily at

this point; it's easy to get rid of abrasive particles, and early films may be worn. As a result, the COF increases or decreases from its initial value. Following this step, the COF settles into a state known as steady-state sliding. Wear mechanisms and the presence of the stick-slip phenomena, which promotes confinement and displacement of wear particles, are responsible for the fluctuations (Mechanism with three bodies) **[134]**. The cross-sectional views of wear tracks formed on AISI 316L steel under various simulated body fluid linear sliding wear conditions at 10m. The width and depth of the wear tracks were prominent, indicating decreased material loss**[134].** Ploughing, cutting, and tiny wedge creation are examples of deformation failure mechanisms that can remove material from a surface via plastic deformation (as expected, given the low H^3/E^2 ratio of 0.001 and 0.0001). Ploughing produces a series of parallel lines due to the mechanical deformation of the softer material. During this process, the material is shifted to the sides, forming peaks as seen in the wear track's edges**.**

Figure 4.15 shows the wear with load against no. of cycle's results of 316L SS, in which Fig. 4.15 (a-c) shows at applied load 10, 20, and 40N, respectively, for bare. It indicates that wear with load is higher at 10N and lower at 20N, while 15min. The ta-coated sample is shown in Fig. 4.15(d-f), with higher wear at 10N and least at 40N. Fig. 4.15 (g-i) shows the results for 30 minutes. Ta coated 316L SS summarizes max. Wear at 10N and min. at 40N, and the same results as predicted for the 60min. Ta coated 316L SS. Ta was first considered a human implant material or a biomaterial because of its superior mechanical qualities and resistance to chemical attack. Because of this, an ASTM consensus standard for unalloyed Ta has been established**[135].** Another study of the bare Ti6Al4V and Ti6Al4V coated with Ta-C coatings is concluded as a sliding cycle function in SBF. Throughout the experiment, the Ti6Al4V exhibits a very changing coefficient curve. The coefficient curves for tantalum carbide coatings with carbon content varied from 54.4

to 74.3 in SBF; conversely, they are highly similar **[136].** Because tantalum can establish stable chemical interactions with C atoms, Ta_2O_5 has better adhesion properties. In contrast, due to the limited carbide-forming capacity of chromium and ions, the 316L with a diamond-like coating (DLC) has the worst adhesion. Coating spallation is the failure mode of the 316L/DLC and Co-Cr-Mo/DLC in the friction test **[137].** Because of its strong adhesion, Ta-coated 316L SS has the best wear resistance. When the coating of the particle with different alloys like Ni using PVD, the bonding is improved, and Ni coating on particles offers consistent wear resistance over a wide range of SiC concentrations, while uncoated particles exhibit a significant reduction in wear resistance **[153].** The substrate surface's texture is an important factor in the adhesion of coatings that depend on mechanical bonding to the surface. The substrates are textured in these contexts so that the coating can "grip" onto the surface. A scratch test is used to evaluate substrate and coatings based on a literature review. The coating-substrate combination's mechanical strength (adhesion, cohesion) determines the critical loads **[153].** According to the literature review, Ta coating (10 min) comprises a thin diffusion layer and the loose, brittle β-Ta phase. The coating delamination under the loading force during the friction process is due to the low adhesion and the brittle phase of β-Ta, Fe Ta, and Fe_2Ta. These peeling components then intensify the coating delamination as hard grinding particles. The continuation of this process reduces the coating's resistance to wear and enhances the friction coefficient **[153].**

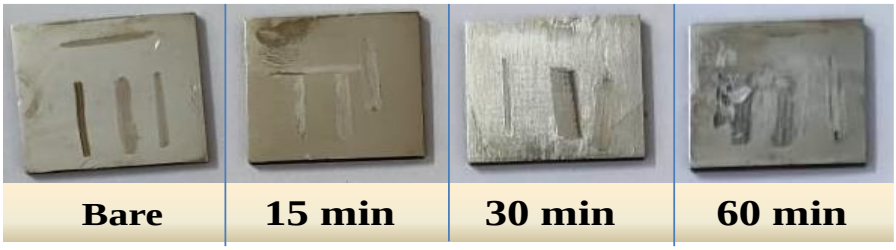

Fig. 4.13 Experimental wear test images of worn surfaces of bare and Ta-coated 316L SS

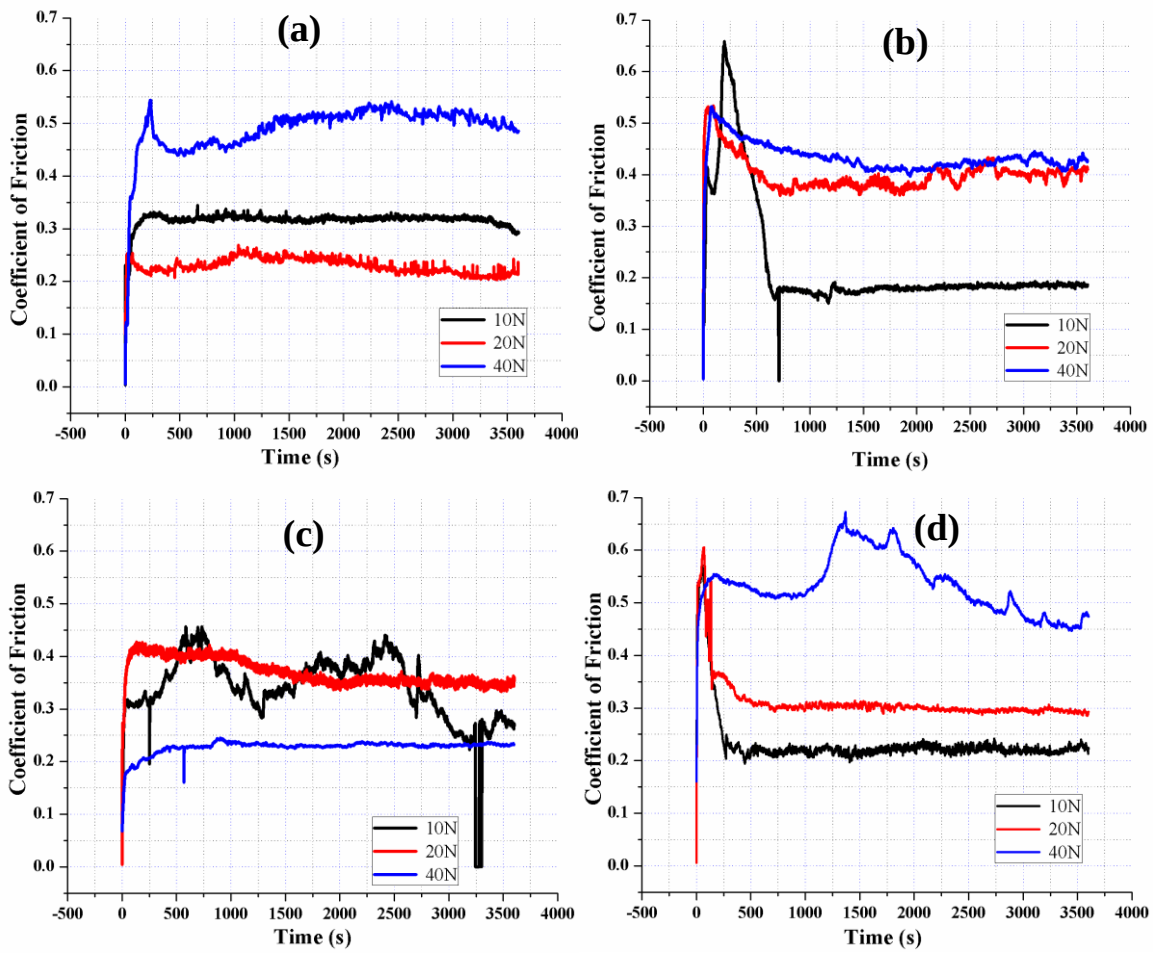

Fig. 4.14 Coefficient of friction against time results of 316L SS; (a) Bare, (b) Ta-coated for 15min., (c) Ta-coated for 30min, and (d) Ta-coated for 60min.

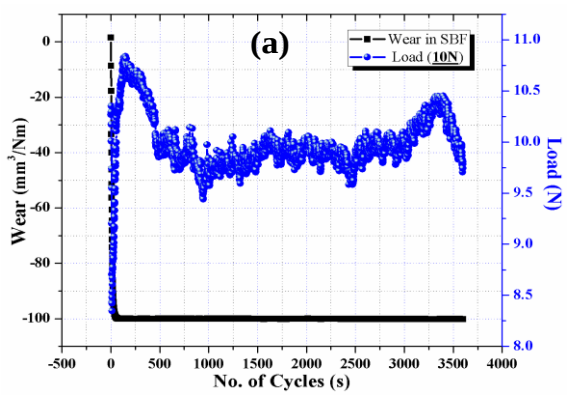
(a)
Wear in SBF
Load (10N)
Wear (mm³/Nm)
Load (N)
No. of Cycles (s)

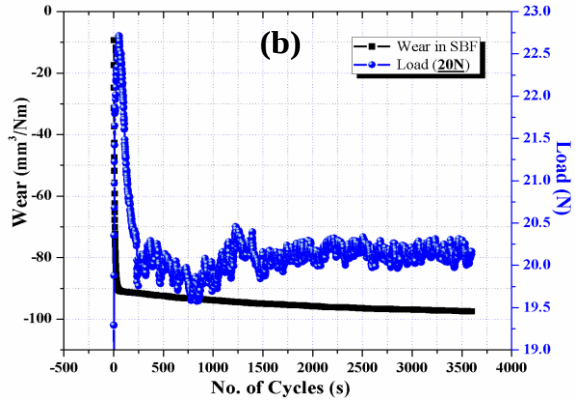
(b)
Wear in SBF
Load (20N)
Wear (mm³/Nm)
Load (N)
No. of Cycles (s)

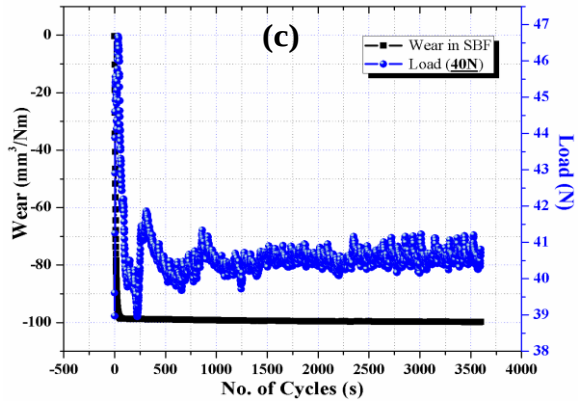
(c)
Wear in SBF
Load (40N)
Wear (mm³/Nm)
Load (N)
No. of Cycles (s)

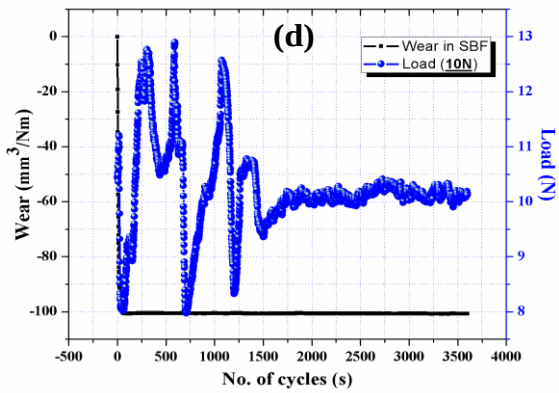
(d)
Wear in SBF
Load (10N)
Wear (mm³/Nm)
Load (N)
No. of cycles (s)

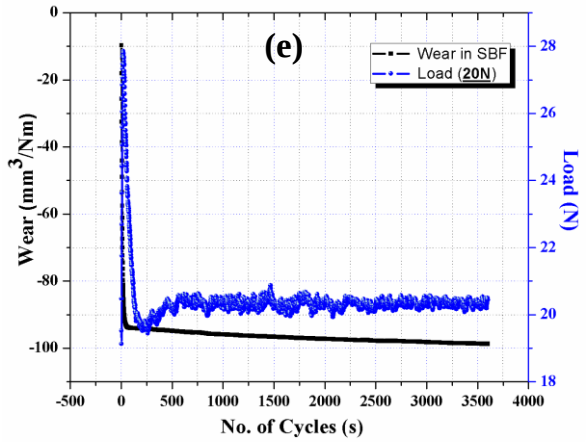
(e)
Wear in SBF
Load (20N)
Wear (mm3/Nm)
Load (N)
No. of Cycles (s)

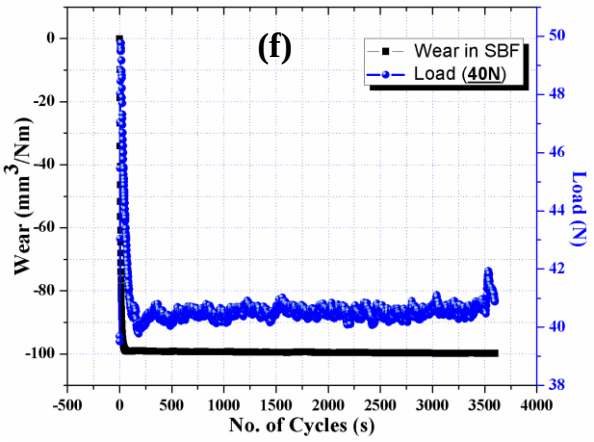
(f)
Wear in SBF
Load (40N)
Wear (mm3/Nm)
Load (N)
No. of Cycles (s)

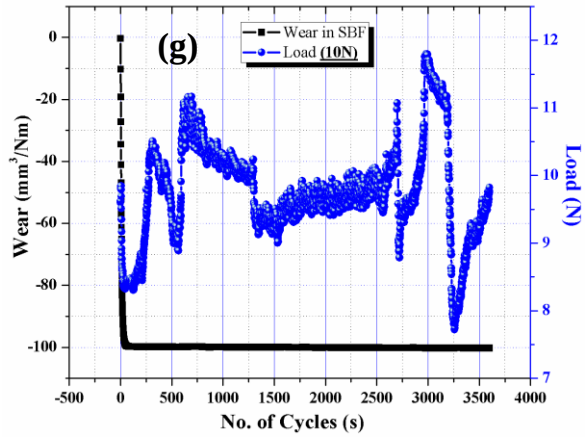
(g)
Wear in SBF
Load (10N)
Wear (mm3/Nm)
Load (N)
No. of Cycles (s)

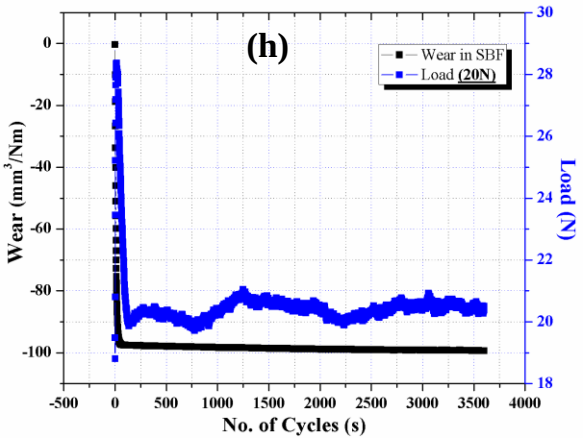
(h)
Wear in SBF
Load (20N)
Wear (mm3/Nm)
Load (N)
No. of Cycles (s)

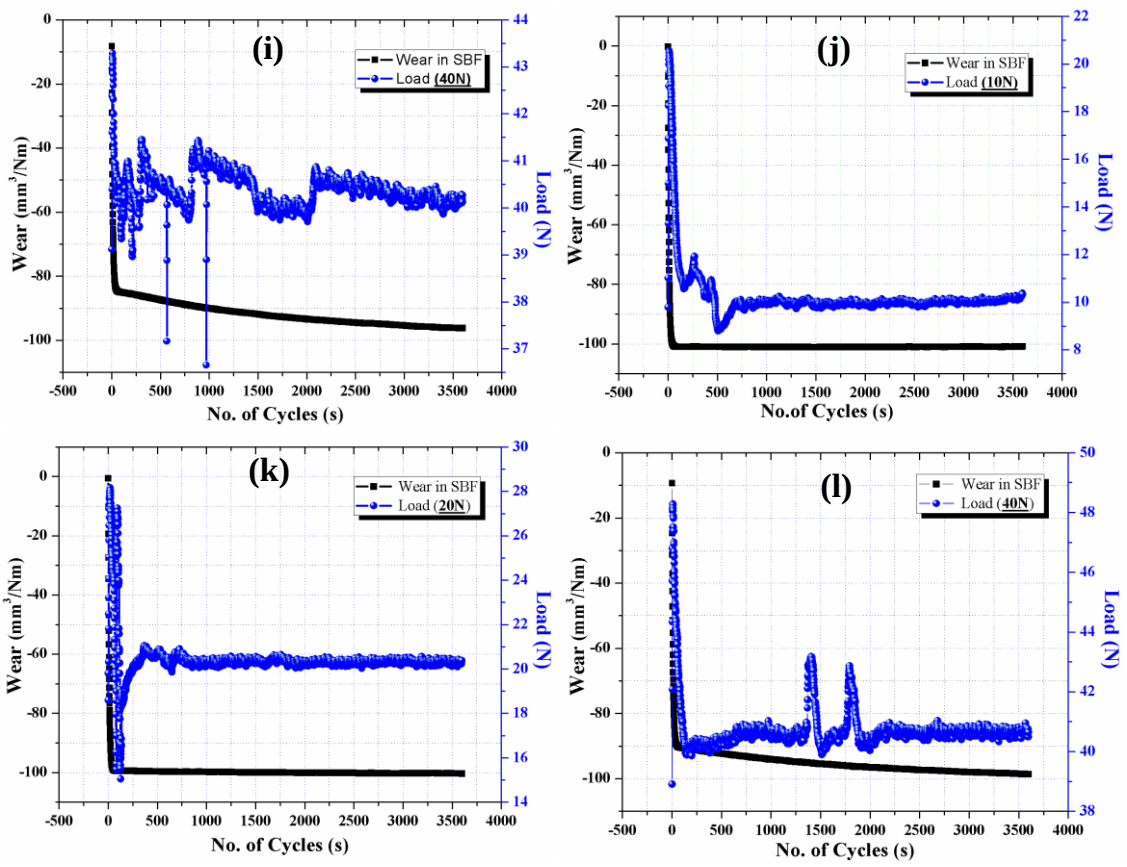

Fig. 4.15 Wear with load against no. of cycles results of 316L SS; **(a-c)** Bare 10N, 20N, and 40N, **(d-f)** Ta-coated for 15min. 10N, 20N, and 40N, **(g-i)** Ta-coated for 30min. 10N, 20N, and 40N, **(j-l)** Ta-coated for 60min. 10N, 20N, and 40N.

The delamination, abrasive, and oxidational wear of the Ta-coated 316L SS for 15 min substrate is the main manifestation of the wear mechanism of Ta coatings deposited in SBF solution, as determined by the analysis above. Furthermore, abrasive wear and oxidational wear of the Ta coating dominate in 316L SS and Ta coatings for 30 min and 60 min. The pores at the Ta/316L SS weaken the coating adhesion, the increased thickness of the Ta coating increases internal stress, and the prolonged deposition time increases interfacial compounds for the Ta coating deposited for 2 hours**[155]**. Therefore, Ta coatings deposited for 30 and 60 minutes may effectively protect 316L SS in SBF solution against wear.

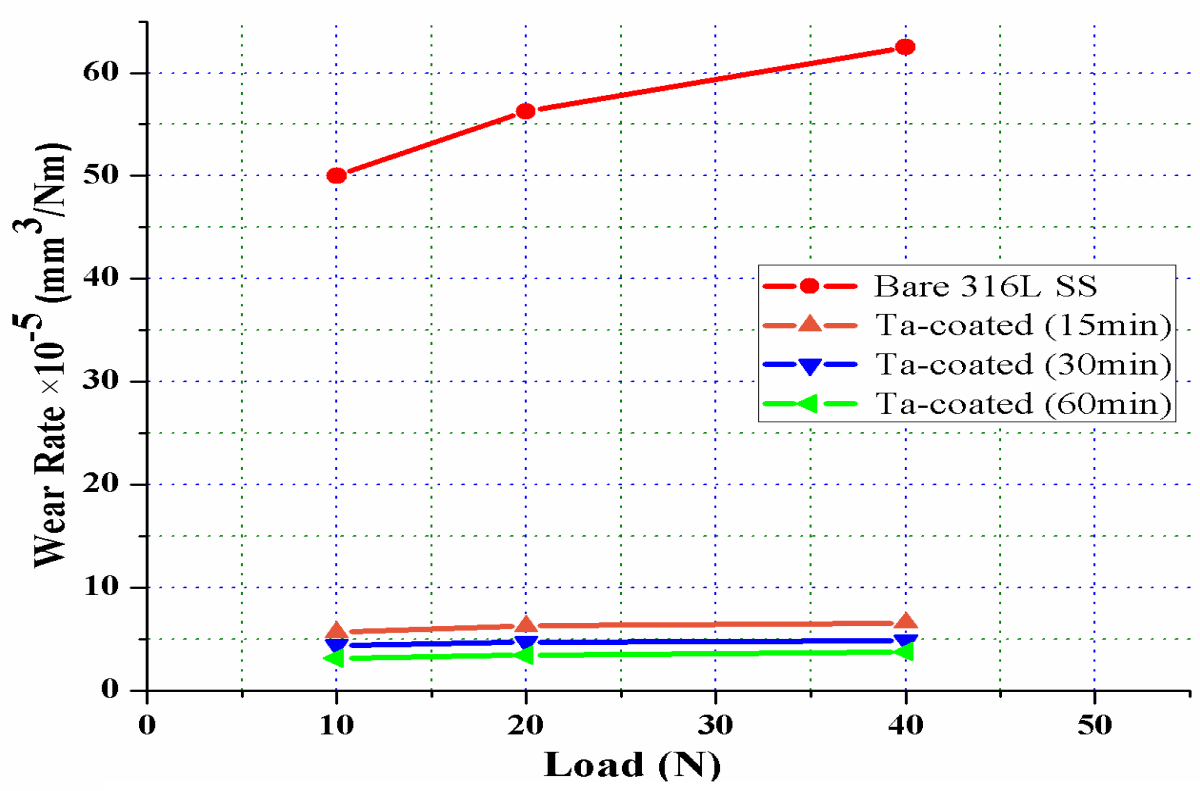

Fig. 4.16 Wear rate against applied load for bare and Ta-coated 316L SS

Fig. 4.16 describes the wear rate against the applied load for bare and Ta-coated 316L SS, clearly indicating the wear rate of the bare sample compared to the Ta-coated samples, which are very high at different loads. Based on the wear test result, the wear rate is calculated as per Archard's equations and obtained that wear rate $\mathbf{(62.50 \times 10^{-5}\, mm^3/Nm)}$ is very high for bare 316L SS at an applied load of 40N, and the wear rate ($\mathbf{3.75 \times 10^{-5}\, mm^3/Nm}$) is low for 60min. Ta-coated 316L SS at the same load.

4.5 Conclusion

The bare 316L SS releases toxic ions into the body due to its poor tribological properties, harming the long-term implant application. To overcome this issue, we applied a thin layer coating of tantalum over the 316L SS with the help of the DC Magnetron Sputtering system for the orthopedic implant. Materials characterization revealed Ta's strong metallurgical adhesion over the 316L SS and confirmed the significant improvement in wear behaviour. The behaviour observed in both samples (bare and coated) under different conditions suggests that the wear mechanism during the test is the same. After Ta-coating on 316L SS, hardness increased to 3783.28 MPa, and modulus of elasticity decreased to **132.16 GPa** against the bare 316L SS. The wear rate of the bare sample is very high $\mathbf{(62.50 \times 10^{-5}\, mm^3/Nm)}$ as compared to Ta-coated 316L SS at an applied load of 40N, while Ta-coated 316L SS for 60 minutes found a very low ($\mathbf{3.75 \times 10^{-5}\, mm^3/Nm}$) wear rate at the same load, Ta-coated have better wear resistance compared to bare 316L SS. The results also confirmed that the wear mechanism in the SBF environment and developed coating is so effective in preventing the wear on the surface of 316L SS that Ta-coating may be recommended as a preferable coating.